Strain relaxation in InNyAs1-y films on (100) GaAs

Wu, X.; Baribeau, J. -M.; Gupta, J. A.; Beaulieu, M.

Publisher's version / Version de l'éditeur:
https://doi.org/10.1016/j.jcrysgro.2005.04.081
Journal of Crystal Growth, 282, 1-2, pp. 18-28, 2005-08-15

Available online at www.sciencedirect.com
SCIENCE DIRECT®
Journal of Crystal Growth 282 (2005) 18–28
JOURNAL OF CRYSTAL GROWTH
www.elsevier.com/locate/jcrysgro

Strain relaxation in GaN_yAs_{1-y} films on (1 0 0) GaAs

X. Wu*, J.-M. Baribeau, J.A. Gupta, M. Beaulieu

Institute for Microstructural Sciences, National Research Council of Canada, Ottawa, Ontario, Canada K1A 0R6

Received 8 October 2004; accepted 22 April 2005
Available online 16 June 2005
Communicated by G.B. Stringfellow

Abstract

The strain relaxation behavior for a series of GaN_yAs_{1-y} films was studied by transmission electron microscopy, high-resolution X-ray diffraction and atomic force microscopy. Samples consisting of 200 nm thick GaN_yAs_{1-y} epitaxial layers with $0.025 \leqslant y \leqslant 0.065$ (i.e. various misfit strain) were grown on (1 0 0) GaAs substrates by molecular beam epitaxy at 460 °C. The $GaN_{0.025}As_{0.975}$ film shows no misfit dislocations and remains pseudomorphic well beyond the Matthews and Blakeslee's critical thickness, which can be explained by the high activation energy for a homogeneous dislocation nucleation at a smooth film surface. In samples with large N content ($y > 0.04$) relaxation of the built-in strain proceeds through morphological changes involving formation of surface cusps, followed by stacking faults and microtwins. The surface nucleation of 90° partial dislocations is shown to be feasible at the low growth temperature in the presence of cusps due to the stress concentration. The surface roughness is anisotropic between the two ⟨0 1 1⟩ directions in the low strained films, and this anisotropy of the surface morphology decreases with increase in N concentration.

PACS: 68.60.Bs; 81.15.Hi; 68.55.−a; 61.16.Bg

Keywords: A1. Strain relaxation; A1. Transmission electron microscopy; A3. Molecular beam epitaxy; B2. Semiconducting III–V materials

1. Introduction

GaN_yAs_{1-y} alloy semiconductors are of technological importance for optoelectronic devices. Recently, there has been considerable interest in using the dilute nitrides as the active materials in semiconductor lasers grown on GaAs substrates. The incorporation of very small amounts of nitrogen into GaAs leads to a dramatic decrease in the bandgap energy and has enabled the growth of GaAs-based laser diodes functioning in the 1.3–1.55 μm range [1,2]. From a purely scientific standpoint, the growth of epitaxial GaN_yAs_{1-y} films on GaAs substrates presents a unique

*Corresponding author. Tel.: +1 613 993 7823; fax: +1 613 952 6337.
E-mail address: xiaohua.wu@nrc.ca (X. Wu).

0022-0248/$ - see front matter
doi:10.1016/j.jcrysgro.2005.04.081

opportunity for studying growth mechanisms and strain relaxation in a highly-mismatched system. The thermodynamic properties of this system have been studied previously, illustrating the wide miscibility gap of the GaN_yAs_{1-y} alloy due to the large difference in the sizes of N and As atoms [3]. In order to avoid phase separation and increase the *N* incorporation, low growth temperatures are used, which pushes the growth process further out of equilibrium.

Although the large miscibility gap and low growth temperature affect the quality of GaN_yAs_{1-y} epitaxial films, the strain relaxation in the GaN_yAs_{1-y} films on GaAs substrates plays an important role in controlling the GaN_yAs_{1-y} film quality as well. In the growth of lattice-mismatched semiconductor materials, the most extensively studied strain relaxation mechanism is plastic flow—the development of misfit dislocations along the substrate film interface and the formation of microtwins [4–6]. Alternatively, a purely elastic strain relaxation mechanism has been demonstrated, both theoretically and experimentally—the strain energy stored in the film can be relaxed by creating surface instabilities [7–10]. A third strain relief mechanism in tensile strained layers is cracking [11,12]. The occurrence of any strain relaxation during the epitaxial growth deteriorates the quality of the films making them unsuitable for device applications.

In this work, we describe the effect of strain on the structural properties of GaN_yAs_{1-y}/GaAs alloys and investigate the strain relaxation mechanisms in this material system. We present the results of transmission electron microscopy (TEM), atomic force microscopy (AFM) and high-resolution X-ray diffraction (HRXRD) investigations of a series of 200 nm thick GaN_yAs_{1-y} films with various *N* concentrations (i.e. various misfit strain) grown on (1 0 0) GaAs substrates by molecular beam epitaxy (MBE) at 460 °C.

2. Experimental procedures

The GaN_yAs_{1-y} samples studied in this work were prepared in a single growth run, where a graded nitrogen composition was obtained by deliberately not using substrate rotation during growth, in order to exploit the natural geometric flux gradients of the MBE system. The nominally 200 nm thick GaN_yAs_{1-y} epilayer was grown on a GaAs (1 0 0) substrate in a custom VG Semicon V90 MBE system. Gallium was provided by a thermal effusion cell, a valved cracker cell was used for As_2 and active nitrogen was provided by an Applied-Epi Unibulb RF plasma cell using dynamic gas switching. Before growth, the native surface oxide was removed by heating the substrate to 630 °C under an arsenic flux, and a 200 nm thick GaAs buffer layer was then grown at 600 °C. The wafer rotation was then stopped and the substrate temperature was lowered to 460 °C for the growth of the GaN_yAs_{1-y} epilayer. The ternary layer was grown at a rate of 1 ML/s, measured at the wafer center, and the As_2 flux was maintained at 1.1 times the flux required for stoichiometric GaAs growth at this rate. The fixed active nitrogen flux at the center of the wafer was selected to provide a number of samples spanning a wide composition range. The wafer was then cleaved along the direction of the nitrogen composition gradient into a set of 5 mm × 10 mm samples and the compositions were estimated by HRXRD. The MBE system is configured so that the Ga flux, and hence growth rate, is approximately constant along the direction of nitrogen gradient. The HRXRD measurements were carried out in a Philips MRD system using Cu $K\alpha_1$ radiation and using a channel-cut Ge(2 2 0) monochromator. The experimental data near the GaAs(4 0 0) reflection were analyzed using dynamical diffraction fitting. X-ray reciprocal space mapping was performed using the $(4\bar{2}\bar{2})$ reflection in a glancing exit geometry with a 0.1° detector acceptance angle. Four pieces of wafer with composition $GaN_{0.025}As_{0.975}$, $GaN_{0.038}As_{0.962}$, $GaN_{0.052}As_{0.948}$ and $GaN_{0.065}As_{0.935}$ were used for this study. ⟨0 1 1⟩ cross-section samples were prepared for TEM following standard procedures and examined in a Philips EM 430 operating at 250 kV and a JEOL JEM 2100F operating at 200 kV. The [0 1 1] and $[0\,\bar{1}\,1]$ directions of (1 0 0) GaAs wafers are given by wafer manufacturer in the wafer specifications. The AFM studies were

performed in air using a Digital Instruments Nanoscope III system.

3. Observations

Fig. 1a is an X-ray reciprocal space map about the $[4\bar{2}\bar{2}]$ reflection for a $GaN_{0.025}As_{0.975}$ sample. The lower peak is the $4\bar{2}\bar{2}$ reflection from the GaAs substrate while the upper peak is the corresponding diffraction peak from the $GaN_{0.025}As_{0.9752}$ epilayer. Both peaks lie on the same vertical line, which indicates that the 200 nm thick $GaN_{0.025}As_{0.975}$ film has retained most of its strain, with its lattice constant in the growth plane closely matching that of the underlying (1 0 0) GaAs substrate. The epilayer peak is broadened and elongated, however, indicating that the film is not a perfect single crystal but is made of crystallites with a finite correlation length (ℓ) parallel to the surface plane and microscopic tilt (δ) perpendicular to the radial direction. The correlation length and tilt are related to the parallel and radial component of the elliptically-shaped Bragg peak (see inset, Fig. 1a) [13]. For this particular film, the long-axis of the ellipse is essentially normal to the radial direction, which indicates a long lateral correlation length. Given the finite diffractometer angular resolution, we can only estimate $\ell \geqslant 0.8\,\mu m$. From the half width of the ellipse, we estimate $\delta \geqslant 0.06^\circ$. Fig. 1b is a bright field $[0\,\bar{1}\,1]$ cross-sectional TEM image of the same sample showing the good crystallinity and an absence of dislocations or other defects in the epitaxial film. No microscopic tilt is apparent in the TEM image due to its limited view area.

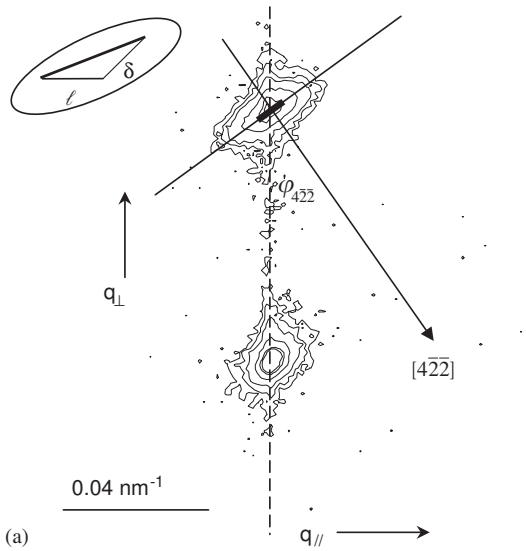

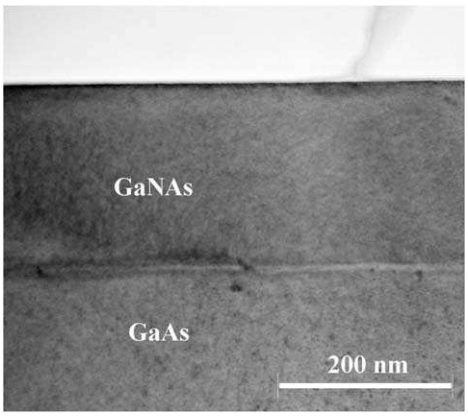

(b)

Fig. 1. X-ray reciprocal space mapping (a) and $[0\,\bar{1}\,1]$ cross-section TEM image (b) of the sample $GaN_{0.025}As_{0.975}$ showing the absence of structural defects in the film.

The surface morphology of three higher N concentration samples $GaN_{0.038}As_{0.962}$, $GaN_{0.052}As_{0.948}$ and $GaN_{0.065}As_{0.935}$ was studied by AFM. Fig. 2 shows the surface morphology changes with the change in N concentration. For the $GaN_{0.038}As_{0.962}$ sample, the surface roughness is anisotropic between the two $\langle 0\,1\,1 \rangle$ directions: the roughness is running predominately along [0 1 1] direction (Fig. 2a). As the N concentration increases, the film surface becomes much rougher, and the anisotropy of the surface morphology between two $\langle 0\,1\,1 \rangle$ directions decreases (Fig. 2b). In the highest N concentration $GaN_{0.065}As_{0.935}$ film, the surface morphology is isotropic between the two $\langle 0\,1\,1 \rangle$ directions and 3-D island growth was observed (Fig. 2c). Similar observations of the surface morphology change with the change in N concentration have been reported in GaAsN films on (0 0 1) GaAs by metalorganic molecular beam epitaxy [14,15]. The anisotropic behavior of the surface morphology between two $\langle 0\,1\,1 \rangle$ directions has also been

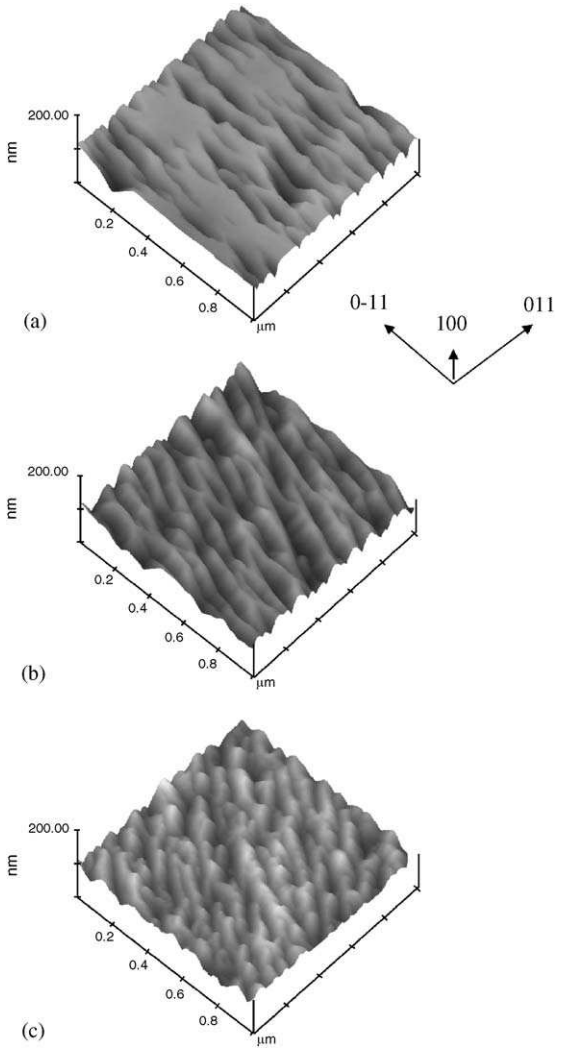

Fig. 2. AFM observations of the surface morphology change with the change in N concentration. (a) $GaN_{0.038}As_{0.962}$, (b) $GaN_{0.052}As_{0.948}$ and (c) $GaN_{0.065}As_{0.935}$ films.

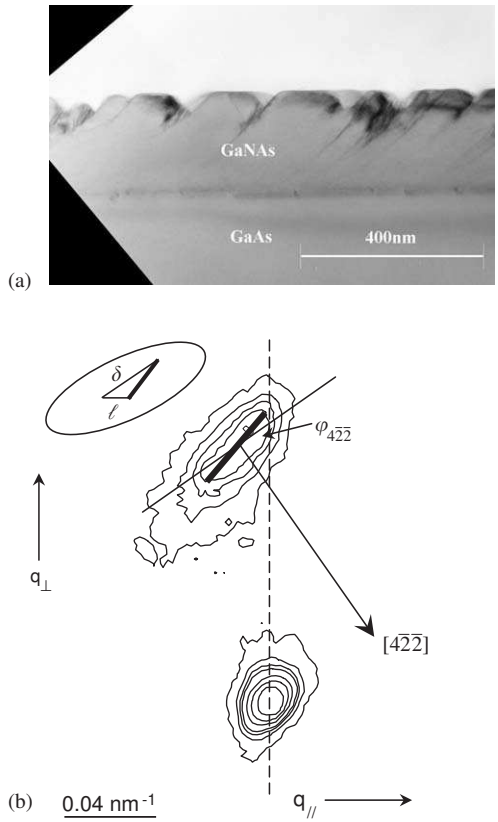

Fig. 3. (a) $[0\,\bar{1}\,1]$ cross-section TEM image showing the cusps in the surface of the $GaN_{0.038}As_{0.962}$ film. (b) X-ray reciprocal space mapping showing the strain relaxation in the film.

observed in InGaAsP films grown on (1 0 0) InP substrates by molecular beam epitaxy [16].

Further structural studies of the three higher N concentration samples were obtained by cross-sectional TEM. Fig. 3a is a bright field $[0\,\bar{1}\,1]$ cross-sectional TEM image of the $GaN_{0.038}As_{0.962}$ sample exhibiting two distinct regions in the film. The first 100 nm of the film is a perfect, defect-free epitaxial layer. Further deposition leads to the formation of cusps in the growing surface and a breakdown of coherent epitaxy. The $[4\,\bar{2}\,\bar{2}]$ reflection X-ray reciprocal space mapping reveals the strain relaxation in the film (Fig. 3b). The GaNAs epilayer peak does not lie on the same vertical line with the GaAs substrate peak, but is shifted towards the bulk alloy lattice constant. From the orientation and half width of the ellipse we estimate $\ell \geqslant 75$ nm and $\delta \geqslant 0.26°$. This correlation length is consistent with the lateral size of the cusped columnar structure of Fig. 3a. The reciprocal space map in Fig. 3b is unusual in that the inclination of the GaNAs ellipse is larger than the normal to the $[4\,\bar{2}\,\bar{2}]$ reciprocal vector. This can be explained by the presence of crystallites with a distribution of lattice constants in the growth direction. It is possible that the lateral size of the columns seen in Fig. 3a influence the lattice strain in the growth direction.

The [0 $\bar{1}$ 1] cross-section TEM image shows that the surface of the $GaN_{0.052}As_{0.948}$ film becomes much rougher (Fig. 4a) compared with lower *N* concentration film $GaN_{0.038}As_{0.962}$ (Fig. 3a). Fig. 4a also indicates a high defect density in the film with cusp formation beginning after the first 25 nm of epitaxial growth. The columnar structure along the ⟨1 1 1⟩ direction is visible in the film. Stacking faults and microtwins (planar defects) are also visible in the film. The highest *N* concentration $GaN_{0.065}As_{0.935}$ film also has many defects as shown in Fig. 4b. For this film, no region is free of defects. The columnar structure is more obvious, and the planar defect density is much higher.

Detailed analysis of the column structure and planar defects were performed by high-resolution TEM (HRTEM) and selected area electron diffraction (SAED). An HRTEM image of the $GaN_{0.065}As_{0.935}$ film shows the column structures with clear boundaries between columns running along ⟨1 1 1⟩ direction (Fig. 5a). Another HRTEM image of the $GaN_{0.065}As_{0.935}$ film shows that planar defects were formed in both (1 1 1) and ($\bar{1}$ 1 1) planes (Fig. 5b). Note that the intersection of (1 1 1) plane and (0 $\bar{1}$ 1) plane is [2 $\bar{1}$ $\bar{1}$], and the

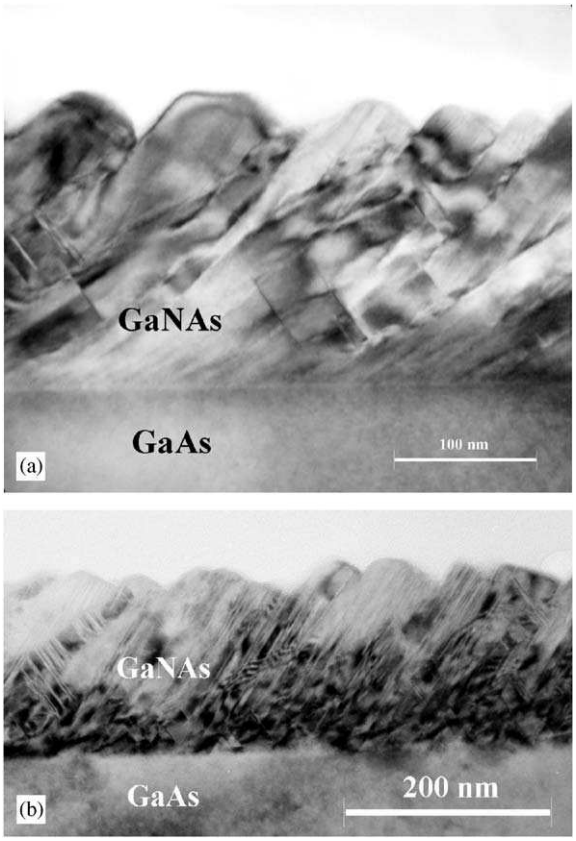

Fig. 4. [0 $\bar{1}$ 1] cross-section TEM images showing the surface, twin and column structures in $GaN_{0.052}As_{0.948}$ (a) $GaN_{0.065}As_{0.935}$ (b) films.

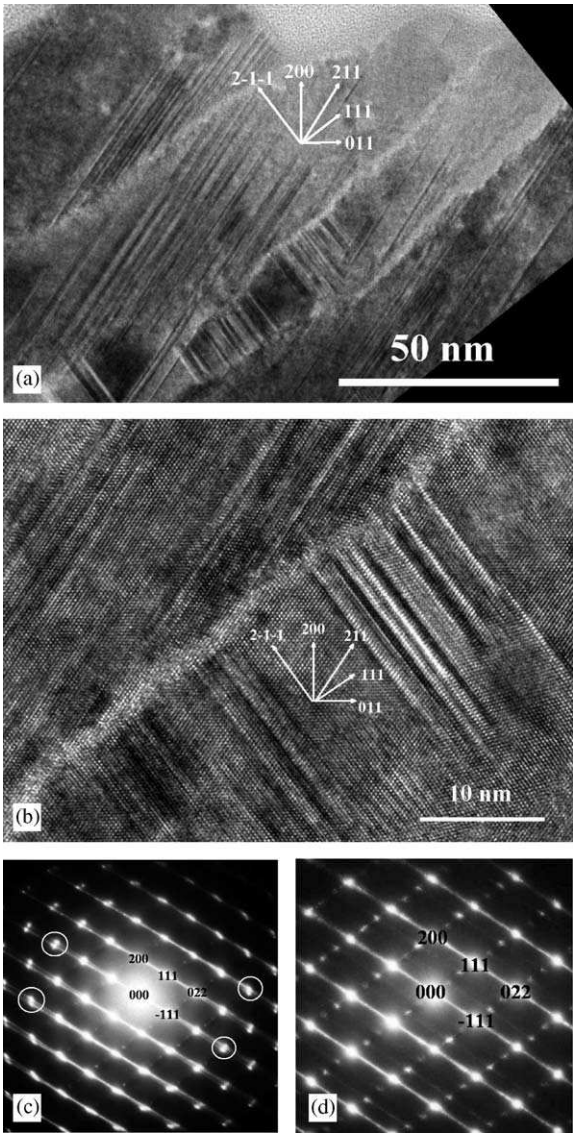

Fig. 5. [0 $\bar{1}$ 1] cross-section HRTEM images and corresponding [0 $\bar{1}$ 1] SAED patterns showing the column structure (a and c) and planar defects (b and d) in the $GaN_{0.065}As_{0.935}$ film.

intersection of $(\bar{1}\,1\,1)$ plane and $(0\,\bar{1}\,1)$ plane is $[2\,1\,1]$, so the planar defects in the $(1\,1\,1)$ and $(\bar{1}\,1\,1)$ planes are running along $\langle 2\,1\,1 \rangle$ directions in the $[0\,\bar{1}\,1]$ cross-section TEM image. Fig. 5c is the SAED pattern from the area shown in Fig. 5a with the electron beam along $[0\,\bar{1}\,1]$ direction, i.e. the specimen is tilted to $[0\,\bar{1}\,1]$ zone axis. The well-defined zinc-blende spots are indicative of the presence of epitaxially grown films. However, the well-defined zinc-blende spots split (some split spots are indicated by white circles in Fig. 5c as examples), which implies that the columns are slightly tilted with reference to each other. Fig. 5d is the SAED pattern from the area shown in Fig. 5b with the electron beam along $[0\,\bar{1}\,1]$ direction. Again, the SAED pattern shows strong $[0\,\bar{1}\,1]$ zone axis diffraction spots from the epitaxial GaNAs layer. The extra weak diffraction spots along $[1\,1\,1]$ direction and lines of diffuse diffracted intensity along $[\bar{1}\,1\,1]$ direction indicate the presence of planar defects in $(1\,1\,1)$ and $(\bar{1}\,1\,1)$ planes [15,17].

The core structures (lower ends) of the planar defects were studied by HRTEM as well. Fig. 6a is a HRTEM image of the core structure of a planar defect. This planar defect is associated with a single partial dislocation in the lower end. The fast Fourier transform (FFT) image of Fig. 6a is shown in Fig. 6b and c is the inverse fast Fourier transform (IFFT) image formed using $\{1\,1\,1\}$ and $\{2\,0\,0\}$ reflections from the FFT image. According to the right-hand/start-finish convention, a Burgers circuit constructed around the lower end of the planar defect is also shown in Fig. 6c. The Burgers vector is determined to be $(a/6)[2\,\bar{1}\,\bar{1}]$. Since $(a/6)[2\,\bar{1}\,\bar{1}]$ is perpendicular to the dislocation line direction $[0\,\bar{1}\,1]$, the $(a/6)[2\,\bar{1}\,\bar{1}]$ dislocation is a 90° Shockley partial dislocation, bounded by a stacking fault lying on the $(1\,1\,1)$ plane. This observation confirms that the 90° Shockley partial dislocation is the leading partial dislocation in a tensile strained epitaxial films, in agreement with earlier studies of tensile strained films [6,18,19]. The stacking fault is formed according to the following reaction in $(1\,1\,1)$ plane:

$$\frac{a}{2}[1\,0\,\bar{1}] \rightarrow \frac{a}{6}[2\,\bar{1}\,\bar{1}] + \text{S.F.} + \frac{a}{6}[1\,1\,\bar{2}],$$

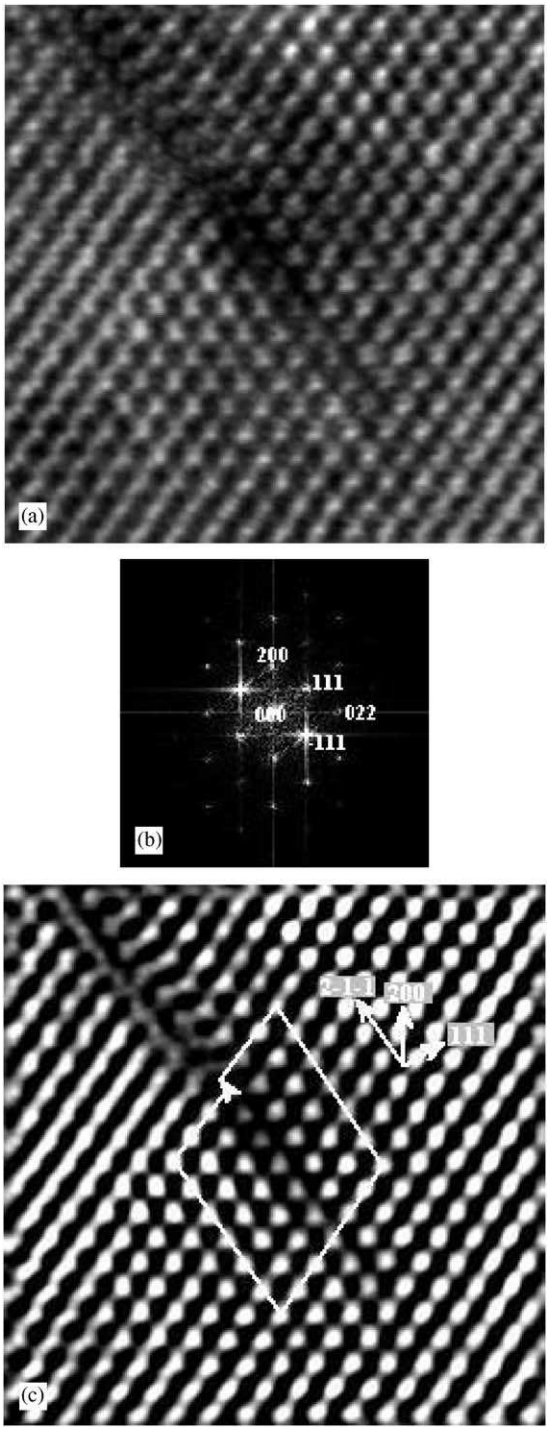

Fig. 6. (a) $[0\,\bar{1}\,1]$ cross-section HRTEM image of the lower end of a planar defect. (b) FFT image. (c) IFFT image with the Burgers circuit showing that the dislocation is a 90° partial dislocation.

where (a/2) [1 0 $\bar{1}$] is a 60° perfect dislocation, (a/6)[2 $\bar{1}$ $\bar{1}$] is a 90° leading partial dislocation, (a/6)[1 1 $\bar{2}$] is a 30° trailing partial dislocation, (note that the line direction of both perfect and partial dislocations is [0 $\bar{1}$ 1]), and S.F. is an intrinsic stacking fault.

4. Discussion

In order to discuss the observed structure changes in relation to the strain relaxation in the films, some of the relevant properties of the cubic zinc blende structure GaN_yAs_{1-y} compounds are summarized in Table 1. The properties of four GaN_yAs_{1-y} films have been estimated from the data for GaAs and GaN, assuming Vegard's law. Vegard's law for any quantity, Q is given by

$$Q_{GaN_yAs_{1-y}} = (1-y)Q_{GaAs} + yQ_{GaN}. \quad (1)$$

The lattice misfit (f) of a GaN_yAs_{1-y} alloy film on a GaAs substrate is defined by

$$f = \frac{a_{GaAs} - a_{GaN_yAs_{1-y}}}{a_{GaN_yAs_{1-y}}} = \frac{1.1499y}{(5.6533 - 1.1499y)}, \quad (2)$$

where a_{GaAs} and $a_{GaN_yAs_{1-y}}$ are the lattice constants of GaAs and GaN_yAs_{1-y}, respectively. Since the lattice constant of the GaN_yAs_{1-y} film is less than that of GaAs, the film is under tension, and the four films in this study have misfit strain of 0.51%, 0.78%, 1.07% and 1.34% respectively according to Eq. (2). The thermal mismatch strain on cooling from the growth temperature to room temperature ($2.27-5.97\times10^{-5}$), is very much smaller than the growth strain ($0.51–1.34\times10^{-2}$), so this effect can be safely ignored.

The Matthews and Blakeslee critical thickness (h_c) for the formation of misfit dislocation for a single epitaxial layer is given by [5]

$$h_c = \frac{b}{8\pi f}\frac{(1-v\cos^2\beta)}{(1+v)\cos\varphi}\left(\ln\frac{h_c}{b}+1\right), \quad (3)$$

where b is the Burgers vector, v is Poisson's ratio, β is the angle between the dislocation line and its Burgers vector and φ is the angle between the slip direction and that direction in the film which is perpendicular to the line of intersection of the slip plane and the interface (or free surface).

In the cubic zinc blende structure, the usual slip systems are $(a/2)\langle 0\,1\,1\rangle$–$\{1\,1\,1\}$. For a lattice mismatched layer grown on a (1 0 0) substrate, $\{1\,1\,1\}$ slip planes make [0 1 1] or [0 $\bar{1}$ 1] intersections with the interface and the most common misfit dislocations are 60° mixed type dislocations with Burgers vector $\mathbf{b} = (a/2)\langle 0\,1\,1\rangle$. In this configuration, $\beta = \varphi = 60°$. For the $GaN_{0.025}As_{0.975}$

Table 1
Properties of GaN_yAs_{1-y} compounds

	GaAs	GaN	$GaN_{0.025}As_{0.975}$	$GaN_{0.038}As_{0.962}$	$GaN_{0.052}As_{0.948}$	$GaN_{0.065}As_{0.935}$
Lattice constant a (Å)	5.6533	4.5034	5.6246	5.6096	5.5935	5.5786
Lattice misfit f (%)	0	25.5	0.51	0.78	1.07	1.34
Shear modulus μ (GPa)	32.5	71	33.5	34.0	34.5	35.0
Poisson's ratio v	0.312	0.366	0.313	0.314	0.315	0.316
Surface energy γ_s (J/m^2) {1 1 0}	0.86	1.97	0.89	0.90	0.92	0.93
Thermal expansion coefficient (10^{-6}/K)	6.0	4.75	6.0	6.0	5.9	5.9
Stacking fault energy (mJ/m^2)	55	22	54	54	53	53

References:
[1] K. Kim, W.R.L. Lambrecht, B. Segall, Phys. Rev. B 53 (1996) 16310.
[2] J.E. Northrup, J. Neugebauer, Phys. Rev. B 53 (1996) R 10477.
[3] Properties of Group III nitride, in: J.H. Edgar (Ed.), Electronic Materials Information Services (EMIS) Datareviews Series Institution of Electrical Engineers, London, 1994.
[4] S. Adachi, 1982 J. Appl. Phys. 53, 8775.
[5] C. Messmer, J.C. Bilello, J. Appl. Phys. 52 (1982) 4623.
[6] K. Suzuki, S. Takeuchi, Phil. Mag. Lett. 79 (1999) 423.
[7] H. Gottschalk, G. Patzer, H. Alexander, Phys. Stat. Sol. (a) 45 (1978) 207.

film with 0.51% misfit strain ($f = 0.0051$, $b = |\mathbf{b}| = 3.9772\,\text{Å}$, $v = 0.313$, see Table 1), the critical thickness for the formation of a 60° dislocation is 218 Å obtained using Eq. (3). However, experiment observation shows that the film grows coherently to a thickness of 200 nm (Fig. 1a and b) that is well beyond this critical thickness.

It is very important to note that in their model Matthews and Blakeslee assumed the source of the misfit dislocation was the pre-existing dislocation in the substrates. If dislocations are present in the substrate on which the film is growing, they grow naturally into the epitaxial film and reach the free surface of the film. These are usually referred to as "threading" dislocations. The biaxial stresses due to the lattice mismatch provide a driving force on some threading dislocations and cause them to move in its slip plane. Beyond the critical thickness h_c, the propagation of threading dislocations in the film leaves behind the misfit dislocation lines along the interface, causing overall relaxation of elastic strain in the film. Matthews and Blakeslee's model can adequately explain the formation of the misfit dislocation at the substrate-heteroepitaxial film interface when a film is grown on a dis located substrate. However, the quality of semiconductor wafers has improved significantly since their 1974 work and most semiconductor substrates used nowadays are free of dislocations or with very low dislocation densities. When epitaxial films are grown on macroscopically dislocation-free substrates, threading dislocations are not available to produce the misfit dislocation. Obviously, in the absence of significant dislocations pre-existing in the substrate, there must be a dislocation nucleation stage during the film growth, which is still not clearly understood. Most studies agree that the nucleation of half-loops of faulted and perfect dislocations (assisted by thermal fluctuation) at the free surface of the growing film is a most probable phenomenon [6,18–20], and nucleation of a 90° partial dislocation with a stacking fault is easier than that of 60° perfect dislocation in 2% tensile strained layers [6]. If the surface of the growing film is flat the change in energy on the introduction of a dislocation half-loop of radius r in a strained layer is given by

$$\Delta E = \left[\frac{\mu b^2 r(1-v/2)}{4(1-v)}\right] \ln\left(\frac{\alpha r}{b}\right) \pm 2rb\gamma_s \sin\theta \pm \frac{1}{2}\pi r^2 \gamma_{S.F.} - \frac{1}{2}\pi r^2 \tau b, \quad (4)$$

where μ is the shear modulus, α is a parameter that related to the dimensions of the dislocation core, γ_s is the surface energy, θ is the angle between the dislocation Burgers vector and the line of intersection of the slip plane and the free surface, $\gamma_{S.F.}$ is the stacking fault energy, and τ is the shear stress on the plane of the dislocation loop. τ is related to the biaxial tensile stress σ by the Schmid factor $\tau = \sigma \cos\phi \cos\lambda$, where ϕ is the angle between σ and the slip plane normal, and λ is the angle between σ and the slip direction. The biaxial stress in the film (σ) is given by $2\mu(1+v)f/(1-v)$, where f is the misfit.

The first term on the right-hand side of Eq. (4) is the self-energy of a dislocation half-loop, taking into account the effects of the free surface, while the fourth term is the strain energy released by the loop, i.e. the work done by the shear stress (τ). The second and third terms represent the energies associated with the formation (annihilation) of surface steps, and the formation (annihilation) of a stacking fault. In the analysis that follows a surface step is assumed to be annihilated, so the negative sign is used in this case for the second term. The third term does not apply when a perfect (60°) dislocation is nucleated, while it gives a positive contribution if a partial dislocation is formed.

Fig. 7 is a plot of ΔE vs. r for a 90° partial dislocation nucleation in the $GaN_{0.065}As_{0.935}$ film with 1.34% misfit strain for a flat surface. Also included in the plot is ΔE vs. r for a cusped surface discussed later. ΔE initially increases with increasing r, reaches a maximum value of ΔE_c (the activation energy for nucleation) at a critical radius r_c, and then decreases as r increases beyond r_c. Table 2 summarizes the values of r_c and ΔE_c for the four films in this study for both 60° and 90° dislocations assuming $\mathbf{b}_{60°} = (a/2)[1\,0\,\bar{1}]$, $\mathbf{b}_{90°} = (a/6)[2\,\bar{1}\,\bar{1}]$, and both dislocations are in (1 1 1) plane. The value $\alpha = 4$ is used for the calculation [21]. A

plot of activation energy (ΔE_c) for the dislocation nucleation vs. misfit (f) (i.e. N concentration) is shown in Fig. 8. The activation energy decreases dramatically with increasing misfit. For a film with misfit $f < 0.6\%$, a 60° dislocation should be formed first, while a 90° dislocation should be formed first in a film with misfit $f > 0.6\%$. However, the most important conclusion from this calculation is that even for the most highly-strained film ($f = 1.34\%$), the activation energy for the dislocation is well above the available free energy of 50 kT from thermal fluctuations [22], which at growth temperature of 460 °C is only 3.16 eV. The activation energy is too high for a homogeneous nucleation process to occur at a flat surface, which could explain the perfect epitaxial growth of the film well beyond the Matthews and Blakeslee's critical thickness for the $GaN_{0.025}As_{0.972}$ film (Fig. 1).

We noted that cusps were formed before any plastic relaxation occurs in the films. The cusps were formed to relieve part of the misfit strain through the "so-called" elastic strain relaxation mechanism [7–10]. For the cusped surface, the stress concentration occurs at the nearly-cusped groove valley and can magnify the stress by a factor of 2–3 [9]. The activation energy for the formation of 90° partial dislocation with a stacking fault in $GaN_{0.065}As_{0.935}$ film is reduced to 2.96 eV from 32 eV if we assume the stress is $2.6\sigma = 2.6 \times 2\mu(1+\nu)f/(1-\nu)$ for the fourth term in the Eq. (4) (Fig. 5). This activation energy is lower than the available thermal free energy 3.16 eV. Thus, for the cusped film, thermal

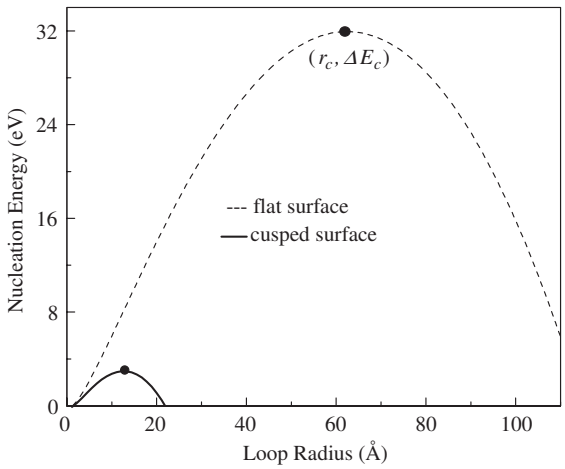

Fig. 7. The variation in ΔE with half-loop radius r in $GaN_{0.065}As_{0.935}$ film for a flat surface and a cusped surface with stress concentration.

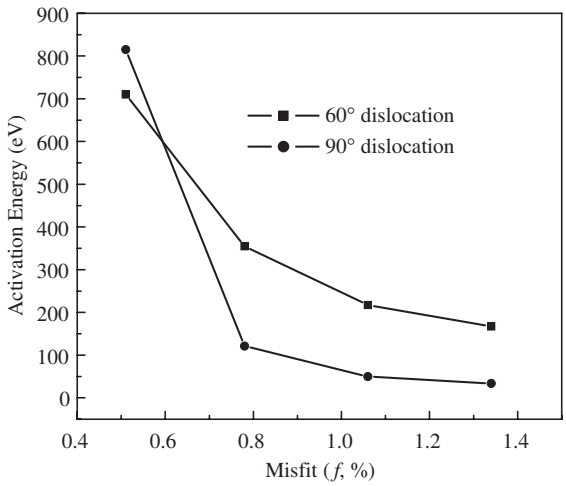

Fig. 8. Activation energy (ΔE_c) for 60° and 90° dislocation nucleation vs. misfit (f).

Table 2
Values of critical radius (r_c) and activation energy (ΔE_c)

Parameter	$GaN_{0.025}As_{0.975}$	$GaN_{0.038}As_{0.962}$	$GaN_{0.052}As_{0.948}$	$GaN_{0.065}As_{0.935}$
b (60° perfect) (Å)	3.9772	3.9666	3.9552	3.9447
b (90° partial) (Å)	2.2962	2.2901	2.2835	2.2774
r_c (Å) (60° perfect)	311	186	128	95
ΔE_c (eV) (60° perfect)	690	369	230	159
r_c (Å) (90° partial)	782	188	94	62
ΔE_c (eV) (90° partial)	723	130	55	32

fluctuations could provide sufficient energy to nucleate a 90° dislocation half-loop. After the first 90° leading partial dislocation bounded by a stacking fault is formed on the {1 1 1} glide plane, a second 90° leading partial dislocation half-loop may be nucleated on neighboring {1 1 1} planes and expand to relax the misfit strain. In this way, stacking faults form sequentially on parallel {1 1 1} planes and produce a microtwin band. The nucleation of 90° partial dislocations on neighboring planes will stop when the stress falls below the critical value needed for nucleation.

The structures observed in this study show some low-temperature MBE growth features such as surface roughening, the formation of planar defects, columnar structure, and amorphous phases. In low-temperature MBE homoepitaxial growth of Si, Ge and GaAs films [23], four distinct stages were observed with the increasing film thickness: (i) perfect, defect-free epitaxial layer, (ii) cusps formation, (iii) stacking faults and microtwins formation and (iv) amorphous phases formation. The mechanisms for the formation of these similar structures are different. In the heteroepitaxial strained layers, the driving force for the formation of the rough growing surface is lattice misfit strain between the film and the substrate, while it is the Ehrlich–Schwoebel diffusion barrier that drives the film to the non-flat surface (kinetic surface roughening) in the low-temperature homoepitaxial films. In order to relieve the misfit strain in the heteroepitaxial layer, the nucleation of a 90° partial dislocation with a stacking fault occurred, and the successive nucleation and glide of 90° partial dislocation on (1 1 1) planes form the twins (so-called deformation twins/stacking faults), while planar defects in low-temperature films are growth twins/stacking faults, and they are formed due to the errors in the sequence of the adatoms arriving on the surface. In the MBE growth of InN_yAs_{1-y} films on GaAs substrate, the relatively low temperature (460 °C) is used to avoid the phase separation and increase the *N* incorporation. We believe this relatively low growth temperature (460 °C) plays a role in the formation of the observed structures in these films.

The formation of the column structure is thought to be the results of evolution of the film growth surface. The cusps are first formed in order to relieve the misfit strain in the heteroepitaxial GaNAs films. When the film is getting thicker, the surface becomes rougher, and islands are formed. As growth continues, boundaries between the islands are formed, and become deeper and wider. It is not clear at this stage why the columns are aligned approximately along ⟨1 1 1⟩ direction (Fig. 5a and b). After the cusps are formed, the 90° partial dislocation half-loop nucleates at the surface sites with the stress concentration due to the presence of cusps as discussed earlier. Normally, the 90° partial dislocations glide on {1 1 1} slip plane after the nucleation and terminate at the thin film-substrate interface in order to effectively relieve the misfit strain in the film. In this study, however, most planar defects are terminated in the middle of the films. This is because the planar defects are confined by the column boundaries. The glide of the 90° leading partial dislocations is stopped by the column boundary, not the film-substrate interface. Fig. 5a clearly demonstrates that the lower ends of the planar defects are terminated in the column boundaries, which results in the termination of the planar defects in the middle of the films.

The anisotropic behavior of the surface morphology between two ⟨0 1 1⟩ directions has been reported in GaAsN films on (0 0 1) GaAs by metalorganic molecular beam epitaxy [14,15], and in InGaAsP films on (1 0 0) InP substrates by molecular beam epitaxy [16]. The anisotropy surface undulation observed in III–V epitaxial layers is believed to be related to surface reconstruction. It is well known that (1 0 0) surfaces of III–V semiconductors are usually reconstructed, e.g. the (2 × 4) reconstruction, so that the directions that were crystallographically equivalent before reconstruction are no longer so after reconstruction. A (Ga)- and B (As)-type steps running along [0 1 1] and [0 $\bar{1}$ 1] directions on a vicinal (1 0 0) reconstructed surface have different characteristics, leading to anisotropic surface diffusivity [24,25]. The diffusion coefficient along [0 $\bar{1}$ 1] direction is four times larger than that of [0 1 1] direction. These factors are believed to contribute also to the anisotropy of surface undulations between two ⟨0 1 1⟩ directions and

explain the roughness is running predominately along [0 1 1] direction. The reason why this anisotropy eventually disappears with the increase in the strain of the film might be related to another surface reconstruction that comes into play at higher strains. Also for more highly-strained films, strain relaxation occurred at the early stage of the film growth, and the film growth continued on the defect surface with cusps and twins, which could contribute to the gradually disappearance of the anisotropy of the surface morphology in higher strained films.

5. Conclusions

We have presented a study of the strain relaxation mechanisms occurring in tensile-strained GaN_yAs_{1-y} films grown in GaAs(1 0 0) for several nitrogen compositions, y. The lowest-composition, $GaN_{0.025}As_{0.975}$ film was epitaxial grown well beyond the Matthews and Blakeslee's critical thickness without misfit dislocations. This phenomenon can be explained by the high activation energy for a homogeneous dislocation nucleation at a flat surface. In films with higher N content ($y > 0.04$) relaxation of the misfit strain proceeds through morphological changes involving formation of surface cusps, followed by stacking faults and twins. The surface nucleation of 90° partial dislocations in the presence of surface cusps was shown to be feasible at the growth temperature due to the stress concentration. The structures observed in the GaN_yAs_{1-y} films were similar to those observed in low-temperature MBE growth of other materials, and were formed in this case because of the strain relaxation in the films. The surface roughness is anisotropic between the two $\langle 0\,1\,1 \rangle$ directions in the $GaN_{0.038}As_{0.962}$ film. This anisotropy of the surface morphology decreases with the increase in N concentration in the films, and disappears in the $GaN_{0.065}As_{0.935}$ film.

References

[1] S.H. Wei, A. Zunger, Phys. Rev. Lett. 76 (1996) 664.
[2] M. Fischer, M. Reinhardt, A. Forchel, Electron Lett. 36 (2000) 1208.
[3] J.A. Gupta, W.R. McKinnon, J. Noad, D. Coulas, R.L. Williams, R. Driad, S.P. McAlister, J. Crystal Growth 231 (2001) 48.
[4] F.C. Frank, J.H. van der Merwe, Proc. R. Soc. A 198 (1949) 216.
[5] J.W. Matthews, A.E. Blakeslee, J. Crystal Growth 27 (1974) 118.
[6] X. Wu, G.C. Weatherly, Phil. Mag. A 81 (2001) 1489.
[7] D.J. Srolovitz, Acta Metall. 37 (1989) 621.
[8] J. Grilhe, Acta Metall. Mater. 41 (1993) 909.
[9] H. Gao, J. Mech. Phys. Solid 42 (1994) 741.
[10] T. Okada, G.C. Weatherly, D.W. McComb, J. Appl. Phys. 81 (1997) 2185.
[11] J.W. Matthews, E. Klokholm, Mat. Res. Bull. 7 (1972) 213.
[12] X. Wu, G.C. Weatherly, Acta Mater. 47 (1999) 3383.
[13] P. Fewster, X-ray Scattering from Semiconductors, Imperial College Press, London, 2000, p. 287.
[14] I. Suemune, N. Morooka, K. Uesugi, Y.-W. Ok, T.-Y. Seong, J. Crystal Growth 221 (2000) 546.
[15] Y.-W. Ok, C.-J. Choi, T.-Y. Seong, K. Uesugi, I. Suemune, J. Electron. Mater. 30 (2001) 900.
[16] X. Wu, G.C. Weatherly, J. Crystal Growth 233 (2001) 88.
[17] P. Hirsch, A. Howie, R.B. Nicholson, D.W. Pashley, M.J. Whelan, Electron Microscopy of Thin Crystals, Krieger, Malabar, Florida, 1977, p. 141.
[18] P.M.J. Maree, J.C. Barbour, J.F. van der Veen, K.L. Kavanagh, C.W.T. Bulle-Lieuwma, M.P.A. Viegers, J. Appl. Phys. 62 (1987) 4413.
[19] J. Zou, D.J.H. Cockayne, J. Appl. Phys. 74 (1993) 925.
[20] V. Kamat, J.P. Hirth, J. Appl. Phys. 67 (1990) 6844.
[21] J.P. Hirth, J. Lothe, Theory of Dislocations, Wiley, New York, 1982, p. 231.
[22] J.W. Matthews, A.E. Blakeslee, S. Mader, Thin Solid Films 33 (1976) 253.
[23] K.A. Bratland, Y.L. Foo, J.A.N.T. Soares, T. Spila, P. Desjardins, J.E. Greene, Phys. Rev. B 67 (2003) 125322.
[24] Y. Horikoshi, H. Yamaguchi, F. Briones, M. Kawashima, J. Crystal Growth 105 (1990) 326.
[25] K. Ohta, T. Kojima, T. Nakagawa, J. Crystal Growth 95 (1989) 71.